energies

MDPI

Article

Basic Characteristics and Design of a Novel Hybrid Magnetic Bearing for Wind Turbines

Yanjun Yu *, Weiyu Zhang, Yuxin Sun and Peifeng Xu

School of Electrical and Information Engineering, Jiangsu University, Zhenjiang 212013, China; zwy@ujs.edu.cn (W.Z.); syx4461@ujs.edu.cn (Y.S.); xupeifeng80@usj.edu.cn (P.X.)
* Correspondence: yuyanjun@ujs.edu.cn; Tel.: +86-511-8879-1245

Academic Editor: Frede Blaabjerg
Received: 8 September 2016; Accepted: 20 October 2016; Published: 2 November 2016

Abstract: This paper proposes a five-degree-of-freedom (5-DOF) hybrid magnetic bearing (HMB) for direct-drive wind turbines, which can realize suspension in the 4-DOF radial and 1-DOF axial directions. Only two sets of radial control windings are employed in the proposed HMB because only one set of radial control windings can achieve the 2-DOF suspension in the radial direction. Unlike the traditional active thrust magnetic bearings, this paper uses a cylindrical rotor core without a large thrust disc in the novel HMB. The numbers of the controller, power amplifier and system volume can be reduced in the magnetic suspension system. This paper also presents the structure and basic characteristics of the proposed magnetic bearing. A precision equivalent magnetic circuit analysis of the permanent magnet ring and control magnetic field is conducted in this study, in consideration of the non-uniform distribution of magnetic density. Accordingly, the mathematical models, including the suspension force expression, are derived based on the accurate equivalent magnetic circuit. The basic principle of the structure parameter design is presented, based on the given key parameters. The accuracy of the analytical method is further validated by 3D finite element analysis.

Keywords: hybrid magnetic bearing (HMB); radial control windings; cylindrical rotor; equivalent magnetic circuit method; finite element analysis (FEA); magnetic suspension force

1. Introduction

Wind turbines have received extensive attention from all over the world because wind energy is a clean and renewable energy. Because the gear boxes are the key factors of maintenance in the wind power generation systems, so the direct-drive permanent magnet wind power generators with no gear boxes are replacing the traditional wind power generators by the wind power manufactures [1,2]. The traditional direct-drive wind turbines supported by ball bearings have a high wind speed at starting, serious wear and mechanical friction problems, and the utilization rate is really low because of aerodynamics (Betz limit) beyond friction and its consequences. Magnetic bearings have a potential application in wind turbines, because of their advantages, including no friction, no wear, no oil lubrication, no seals, low cost, low loss and long life, among others [3–8].

The wind turbines supported by magnetic bearings have many advantages, which include the following: (a) the utilization rate of wind energy will be improved and the threshold wind speed will be reduced because no contact and friction between the stator and the rotor will occur; (b) the costs, environmental pollution and loss will be reduced because no lubrication is present in the magnetic bearings; and (c) magnetic bearings have high adaptability to extreme climate conditions [9–12].

The magnetic bearings used in wind turbines can be classified into three types as follows: active, passive and hybrid magnetic bearings [13–16]. The active magnetic bearings (AMBs) have suspension forces for the rotor that are generated by the coil currents. The AMBs have high control precision and great bearing capacity. However, the AMB systems are composed of sensors, power electronics

and controllers. The passive magnetic bearings (PMBs) can stabilize the rotor with some degrees of freedom without active control. However, the stability and controllable properties of the PMBs are poor. Hybrid-type magnetic bearings have been proposed to combine the merits of AMBs and PMBs. These bearings are thought to be a valuable bearing type. Accordingly, many kinds of hybrid-type magnetic bearings are used in wind turbines and industrial applications [17,18].

The current magnetic suspension system, which mainly adopts one degree-of-freedom (DOF) in the axial direction and 4-DOF in the radial direction, can achieve the suspension in the 5-DOF. This kind of system is widely employed in many industries, such as in precision machining, aeronautics and astronautics [19,20]. Two 2-DOF magnetic bearings are concurrently controlled to achieve 4-DOF in the radial direction. A 2-DOF magnetic bearing usually needs at least four sets of controllers and power amplifiers. The magnetic suspension system with 4-DOF in the radial direction needs at least eight sets of controllers and power amplifiers. Therefore, the magnetic levitation system has a slightly more complicated structure and a higher power consumption [21]. In addition, the axial length of the rotor will be increased when two 2-DOF magnetic bearings are placed alongside the rotor, thereby leading to a system volume and disturbance increase. The stability and controllability of the upper mentioned system will be more difficult. Meanwhile, the magnetic suspension system with the magnetic bearing uses the thrust disc to achieve the suspension in the axial direction at the present stage. Assembling and disassembling are difficult for this system, because the thrust disc is sandwiched between the stators of the magnetic bearing. Moreover, the thrust disc makes the direct insertion of the rotor shaft into the system difficult. Obtaining the dynamic balance of the rotor shaft before the assembly is also hard. In addition, the rotational speed of the thrust disc is limited [22].

Some kinds of 5-DOF magnetic bearings were proposed by many researchers. A 5-DOF magnetic bearing with symmetric permanent magnets and radial stators at the end of the axial thrust disc on the basis of a 2-DOF magnetic bearing was proposed in [23]. Masuzawa T proposed a 5-DOF magnetic bearing system in the 9th International Symposium on magnetic bearings. The axial and radial control fluxes were provided by the radial control windings, but the control fluxes in the radial and axial direction were coupled. The work in [24,25] proposed a 5-DOF axial force tilting permanent magnet biased magnetic bearing with a split stator.

Accordingly, a novel 5-DOF hybrid magnet bearing (HMB) is proposed in this paper. The 5-DOF HMB can realize the suspension in the 4-DOF radial and 1-DOF axial directions. Only two sets of radial control windings are used in the proposed HMB because a single set of radial control windings can achieve the 2-DOF suspension in the radial direction. The system volume, numbers of controller and power amplifier will then be reduced in the magnetic levitation system. The rotor shaft employing the proposed HMB has a simple columnar shape without a large convexity. As a result, the problems caused by the large thrust disc are resolved. This paper also introduces the basic characteristics of the proposed HMB, then deduces the accurate equivalent magnetic circuit, designs the structure parameters and verifies by a computational check the model of the proposed HMB with the 3D finite element analysis (FEA).

2. Configuration and Operation Principle

2.1. Structure of the 5-DOF HMB

Figure 1 shows the structure and the exploded view of the new type of 5-DOF HMB. The HMB comprises the outer stator core, inner stator core, cylindrical rotor core, shaft, radial magnetized permanent magnet (PM) ring, eight radial control windings, two sets of compensating windings for eliminating the influence of gravity and two axial control windings. Figure 2a shows the cutaway view of the proposed 5-DOF HMB. The PM ring provides the biased fluxes for the HMB. The static suspension force generated by the PM ring will suspend the rotor in a balanced position.

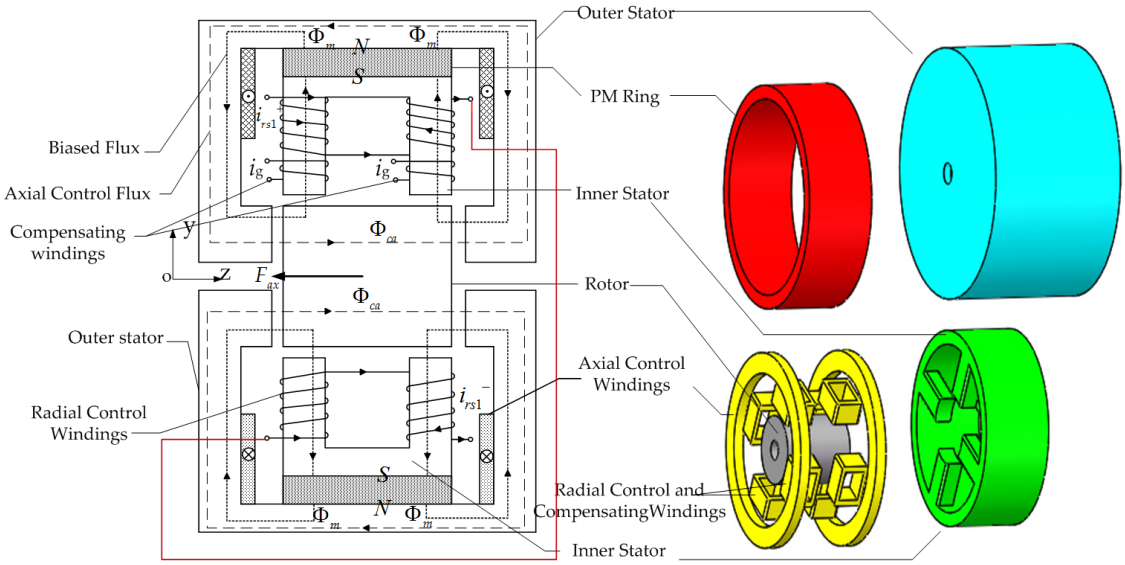

Figure 1. Configuration and the exploded view of the proposed 5-DOF HMB.

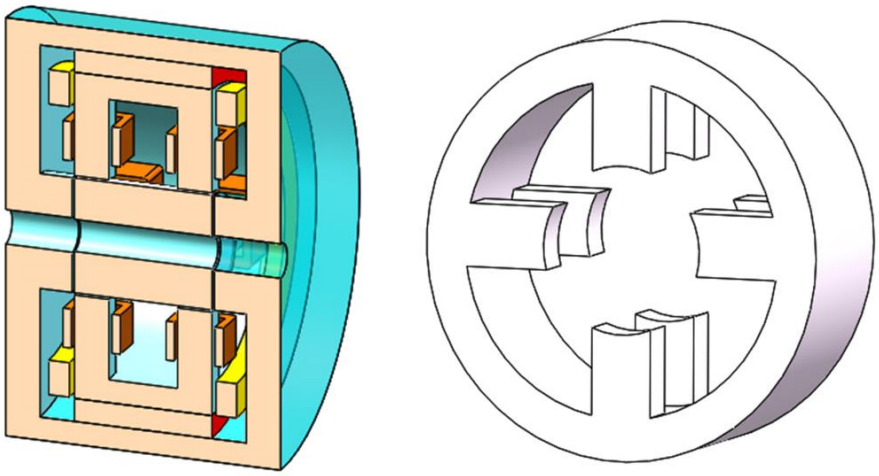

(**a**) (**b**)

Figure 2. The inner stator core and cutaway view of the proposed 5-DOF HMB. (**a**) Cutaway view of the proposed 5-DOF HMB; (**b**) the structure of the inner stator core.

Figure 2b shows the inner stator core made of a cog structure, in which four pairs of inner stator teeth are uniform along the circumference. Two sets of radial control windings are wound on the inner stator teeth. The two axisymmetric radial control windings are connected in series, as shown in Figure 1. The two sets of the radial windings can control the rotor suspension in 4-DOF. The axial control windings distributed around the rotor are wound between the inner stator core and the outer stator core, to achieve a 1-DOF suspension in the axial direction.

Overall, the proposed 5-DOF HMB can simplify the structure and lower the volume compared to the traditional 5-DOF magnetic bearings. Moreover, the novel 5-DOF HMB uses the cylindrical rotor core without the thrust disc in the axial direction. Then, the rotor in this study is further lightened.

2.2. Principle of Radial Suspension Force Generation

The rotor is assumed to be twisted away from the equilibrium position by a disturbance force in the radial direction (Figure 3). The left air gap in the upper rotor lengthens, whereas the right air gap shortens. Consequently, the left air gap in the lower the rotor shortens, whereas the right air gap

lengthens. The current i_{rs1+} is fed into the radial control windings to return to the balance and generate the control flux according to the control demand, as shown in Figure 3. Thus, the control flux will be superposed to the PM-biased flux, which leads to the flux density reduction and increase in the right and left air gaps in the upper rotor. The flux density reduction and increase in the left and right air gaps are also observed in the lower rotor. As a result, the suspension force F_{ra} can lead the rotor to the equilibrium position based on the electromagnetic theory of Maxwell. The principle of the radial suspension force generation in the other two radial DOF is the same as the upper-part.

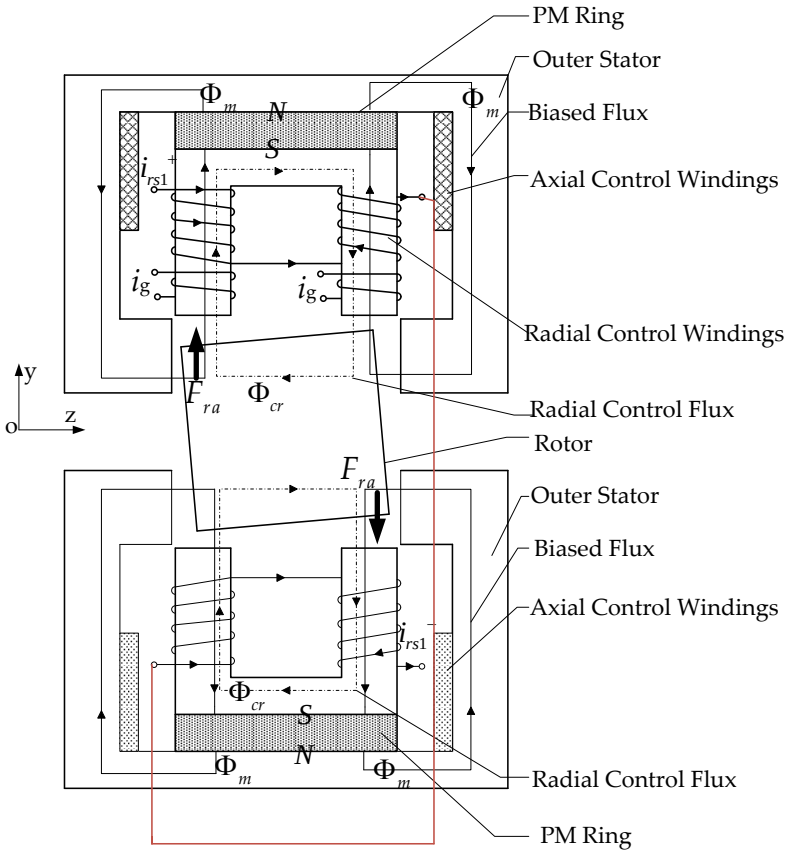

Figure 3. Principle of radial suspension force generation.

2.3. Principle of Axial Suspension Force Generation

Figure 1 shows that the rotor will be displaced from the balance position right when a disturbance force is exerted on the rotor in the axial direction. This action results in the length variation of the air gaps in the axial direction. Consequently, the magnitude of the magnetic flux density in the left air gap around the rotor will be smaller than that in the right. The appropriate currents are fed into axial control windings to return the rotor back to the equilibrium position in the axial direction and generate the control flux Φ_{ca} shown in Figure 1. Thus, the control flux Φ_{ca} can be superposed with the PM-biased flux Φ_m, which leads to the increase of the magnitudes of the magnetic flux density and reduction in the left and right air gaps. The rotor will then be pulled back to the equilibrium position in the axial direction based on the electromagnetic theory of Maxwell.

Therefore, the proposed 5-DOF HMB using the PM-biased flux in this study can achieve the stable suspension of the rotor in 5-DOF.

2.4. Principle of Gravity Compensation

The gravity compensation is necessary due to the gravity of the rotor. Traditionally, there are some ways to compensate the gravity of the rotor, such as by using the asymmetric bias flux; by using

additional passive control windings, etc. Two sets of compensating windings are used in this HMB. As shown in Figure 1, in order to compensate the gravity of rotor, the smaller constant direct current i_g is connected to the two sets compensating windings when the suspension control was acted. Because the gravity of the rotor is much smaller than the external loading, so the compensating current is much smaller than the radial control current. The influence of compensating current on the HBM flux can be ignored in order to simplify the following analysis.

3. Accurate Magnetic Circuit Analysis

Some of the following assumptions are made to simplify the magnetic circulation:

(1) The reluctance of the stator iron core and of rotor core is not considered.
(2) Finite coercivities and magnetic saturation are ignored.
(3) The influence of the compensating current is ignored.

3.1. Accurate Analysis of Equivalent Magnetic Circuit of the PM Ring

The equivalent magnetic circuit will be presented given the flux distribution indicated in Figure 1 and Ohm's law for the equivalent magnetic circuit. The equivalent circuit model of the proposed 5-DOF HMB is shown in Figure 4, because of the symmetry of the PM flux paths. F_m is the magnetic motive force of the PM; Φ_r is the flux source of the PM; Φ_m is the total flux produced by the PM; Φ_1 is the total magnetic flux through the air gap; Φ_{a1} and Φ_{a2} are the air gap fluxes in the left and right parts of the magnetic bearing, respectively. Φ_2 is the magnet-to-magnet leakage flux, which does not produce any active suspension force. R_m is the magnet reluctance of the PM corresponding to Φ_r; $R_{m\sigma}$ is the reluctance caused by the magnet-to-magnet leakage flux Φ_2. R_{ax1} and R_{ax2} are the air gap magnet reluctances in the axial direction corresponding to Φ_{a1} and Φ_{a2}, respectively. R_{ra1} and R_{ra2} are the air gap magnet reluctances in the radial direction corresponding to Φ_{a1} and Φ_{a2}, respectively. The coefficient λ is introduced as follows:

$$\lambda = R_{m\sigma}/R_m \tag{1}$$

The equations of the fluxes are deduced as follows according to Figure 4.

$$\Phi_1 = \frac{\lambda R_m R_\Sigma}{\lambda R_\Sigma R_m + (2+\lambda)(R_{ax1}+R_{ra1})(R_{ax2}+R_{ra2})}\Phi_r \tag{2}$$

where $R_\Sigma = R_{ax1} + R_{ra1} + R_{ax2} + R_{ra2}$:

$$\Phi_{a1} = \frac{R_{ax2}+R_{ra2}}{R_\Sigma}\Phi_1 \tag{3}$$

$$\Phi_{a2} = \frac{R_{ax1}+R_{ra1}}{R_\Sigma}\Phi_1 \tag{4}$$

$$\Phi_m = \frac{\lambda R_m R_\Sigma + 2(R_{ax1}+R_{ra1})(R_{ax2}+R_{ra2})}{\lambda R_m R_\Sigma + (2+\lambda)(R_{ax1}+R_{ra1})(R_{ax2}+R_{ra2})}\Phi_r \tag{5}$$

The magnet reluctances can be written as follows:

$$R_m = \frac{h_m}{\mu_0\mu_r S_m},\ R_{ax1} = \frac{g_0+z}{\mu_0 S_{ax1}},\ R_{ax2} = \frac{g_0-z}{\mu_0 S_{ax2}},\ R_{ra1} = \frac{g_1+y}{\mu_0 S_{ra1}},\ R_{ra2} = \frac{g_1-y}{\mu_0 S_{ra2}} \tag{6}$$

where μ_0 is the permeability of air; μ_r is the relative permeability of PM; and g_0 is the effective widths of the air gap between the rotor and the outer stator teeth in the axial direction when the rotor is in the ideal equilibrium position without external disturbances. g_1 is the effective air length between the rotor and the inner stator teeth in the radial direction when the rotor is not eccentric. x and y are the

eccentricity of the rotor in the axial and radial directions, respectively. S_m is the effective flux passing area of the PM; S_{ax1} and S_{ax2} are the flux passing areas between the outer stator teeth and the rotor in the axial direction. S_{ra1} and S_{ra2} are the flux passing areas between the inner stator teeth and the rotor in the radial direction. The calculations are simplified by assuming that:

$$S_{ax1} = S_{ax2} = S_{ax} \quad S_{ra1} = S_{ra2} = S_{ra} \tag{7}$$

Substituting (7) into (6) and (2) through (5), after some manipulation yields:

$$\Phi_1 = \frac{2\lambda\mu_0 S_{ax} S_{ra} R_m (g_0 S_{ra} + g_1 S_{ax})}{2\lambda\mu_0 S_{ax} S_{ra} R_m (g_0 S_{ra} + g_1 S_{ax}) + (2+\lambda)p} \Phi_r \tag{8}$$

where $p = ({g_0}^2 - z^2){S_{ra}}^2 + 2(g_0 g_1 - yz) S_{ax} S_{ra} + ({g_1}^2 - y^2){S_{ax}}^2$.

If:

$$\beta = \frac{2\lambda\mu_0 S_{ax} S_{ra} R_m (g_0 S_{ra} + g_1 S_{ax})}{2\lambda\mu_0 S_{ax} S_{ra} R_m (g_0 S_{ra} + g_1 S_{ax}) + (2+\lambda)p}, 0 < \beta < 1 \tag{9}$$

then the flux of (8) can be expressed as follows,

$$\Phi_1 = \beta \cdot \Phi_r \tag{10}$$

where:

$$\Phi_r = B_r \cdot S_m \tag{11}$$

The air gap flux can then be obtained as:

$$\Phi_{a1} = \frac{S_{ra}(g_0 - z) + S_{ax}(g_1 - y)}{2(g_0 S_{ra} + g_1 S_{ax})} \Phi_1 \tag{12}$$

$$\Phi_{a2} = \frac{S_{ra}(g_0 + z) + S_{ax}(g_1 + y)}{2(g_0 S_{ra} + g_1 S_{ax})} \Phi_1 \tag{13}$$

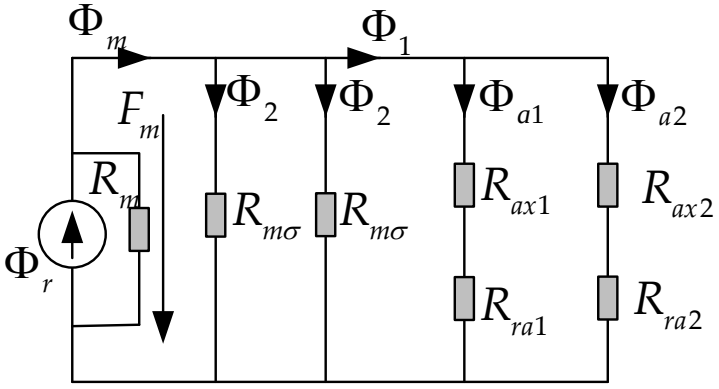

Figure 4. Equivalent magnetic circuit of the PM ring.

The eccentricities z and y in the radial and axial directions are $z = 0$ and $y = 0$, respectively, when no eccentricity happens on the rotor. Figure 5 shows the distribution of the flux density vectors of the PM in the proposed 5-DOF HMB by FEA with no eccentricity.

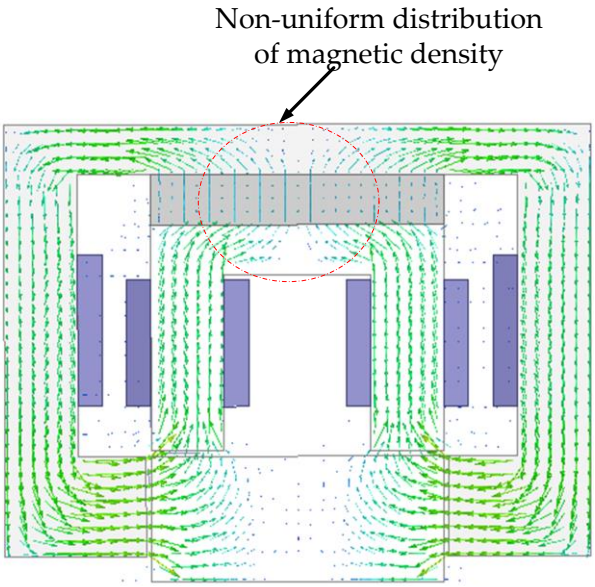

Figure 5. Distribution of flux density vectors of the PM.

As indicated by Figure 5, the flux of the PM flowing from the upper PM ring is divided into the same two tributaries. The tributary flow passes through the outer stator, rotor and inner stator, then returns to the lower PM ring.

The following equation is obtained according to (12) and (13):

$$\Phi_{a1} = \Phi_{a2} = \frac{1}{2}\Phi_1 \tag{14}$$

According to [26], the magnitudes of the intrinsic flux of the PM are equal to the product of a given residual magnetic flux density B_r and the area perpendicular to the magnetic flux density B_r. The distribution of the magnetic density in the upper definition is uniform. Therefore, the area S_m in Equation (11) is the effective area perpendicular to the uniform magnetic flux density B_r. As shown in Figure 5, the magnetic flux density in the upper and lower PM ring is non-uniform. Consequently, a large error will be observed when the actual surface area is directly substituted into the calculating formula. The coefficient α representing the relationship between the effective area of the PM S_m and the actual surface area of the PM, S_{pm} is introduced as follows to reduce the error.

$$\alpha = \frac{S_m}{S_{pm}} \tag{15}$$

The coefficient α in the proposed 5-DOF HMB is set as a constant value, α = 0.83, according to the finite element computations and its results.

Substituting (15) into (10) yields:

$$\Phi_1 = 0.83 \cdot \beta \cdot B_r \cdot S_{pm} \tag{16}$$

3.2. Equivalent Magnet Circuit of the Suspension Control Windings

The flux paths in Figure 3 show two kinds of control magnetic circuits in the magnetic bearing, namely the axial and radial active control circuits. Figure 6 shows the equivalent magnetic circuit model of the two kinds of control magnetic field, where Φ_{ca} and Φ_{cr} are the control fluxes in the axial and radial control circuits, respectively. $N_a i_{ax}$ and $N_r i_{rs}$, ampere-turns, are the magnetomotive forces generated by each control winding.

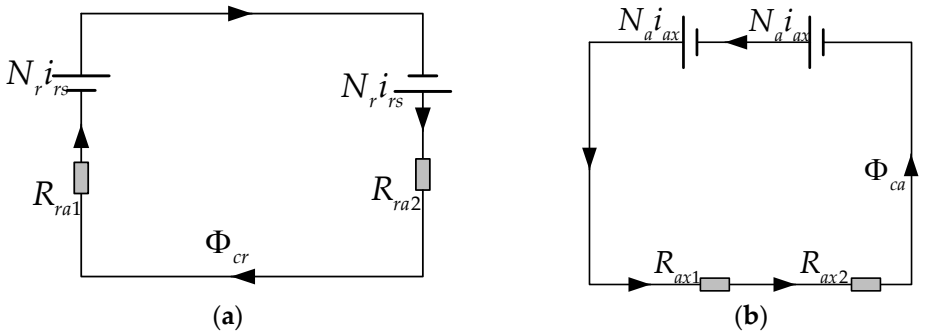

Figure 6. Equivalent magnetic circuit model of control magnetic field. (**a**) The equivalent magnetic circuit model of the radial active control circuit; (**b**) the equivalent magnetic circuit model of the axial active control circuit.

According to Figure 6, the control fluxes can be calculated as follows:

$$\Phi_{cr} = \frac{2N_r i_{rs}}{R_{ra1} + R_{ra2}} \tag{17}$$

$$\Phi_{ca} = \frac{2N_a i_{ax}}{R_{ax1} + R_{ax2}} \tag{18}$$

3.3. Expression of the Suspension Force

The suspension forces in the radial and axial directions can be calculated as follows:

$$F_{ra} = \frac{(\Phi_{a1} + \Phi_{cr})^2 - (\Phi_{a2} - \Phi_{cr})^2}{\mu_0 S_{ra}} \tag{19}$$

$$F_{ax} = 2 \times \frac{(\Phi_{a1} + \Phi_{ca})^2 - (\Phi_{a2} - \Phi_{ca})^2}{\mu_0 S_{ax}} \tag{20}$$

As shown in Figure 3, F_{ra} and F_{ax} are the suspension forces acting on the rotor in the radial and axial directions, respectively. The magnitudes of the biased fluxes in the upper and lower parts of the rotor are similar because of the magnetic bearing symmetry.

Substituting (12), (13), (17) and (18) into (19) and (20) yields:

$$F_{ra} = -\frac{g_0 z {S_{ra}}^2 + S_{ra} S_{ax}(y g_0 + z g_1) + {S_{ax}}^2 g_1 y}{\mu_0 S_{ra}(g_0 S_{ra} + g_1 S_{ax})^2} {\Phi_1}^2 + \frac{2\Phi_1 N_r i_{rs}}{g_1} \tag{21}$$

$$F_{ax} = -\frac{2[g_0 z {S_{ra}}^2 + S_{ra} S_{ax}(y g_0 + z g_1) + {S_{ax}}^2 g_1 y]}{\mu_0 S_{ax}(g_0 S_{ra} + g_1 S_{ax})^2} {\Phi_1}^2 + \frac{4\Phi_1 N_a i_{ax}}{g_0} \tag{22}$$

3.4. Maximum Suspension Force

The following equations can be established according to (19) and (20) to obtain the maximum suspension forces in the radial and axial directions:

$$\Phi_{a1} + \Phi_{cr} = \Phi_{r\max},\ \Phi_{a2} - \Phi_{cr} = 0 \tag{23}$$

$$\Phi_{a1} + \Phi_{ca} = \Phi_{a\max},\ \Phi_{a2} - \Phi_{ca} = 0 \tag{24}$$

where $\Phi_{r\max}$ and $\Phi_{a\max}$ are the maximum resultant magnetic fluxes in the radial and axial directions, respectively. These fluxes are mainly limited by the iron core saturation. Substituting (23) and (24) into (12) and (13) yields:

$$\Phi_{r\max} = \Phi_{a\max} = \Phi_1 \tag{25}$$

The maximum suspension forces can then be deduced as:

$$F_{ra\max} = \frac{{\Phi_1}^2}{\mu_0 S_{ra}} \tag{26}$$

$$F_{ax\max} = 2 \times \frac{{\Phi_1}^2}{\mu_0 S_{ax}} \tag{27}$$

4. Structure Parameter Design

4.1. Magnetic Flux Density in the Air Gap

According to (12), (13), (19) and (20), the maximum force will be generated when the displacement in the radial and axial directions is zero, that is the rotor is at the equilibrium position. The coefficient β can be obtained as setting $\beta \approx 0.96$ because of the leakage flux of the PM ring in the air gap and through the FEA.

The magnetic flux density $B_{r\max}$ in the air gap in the axial and radial directions is set to be 1.5 T considering the magnetic saturation of the silicon steel.

The suspension force is determined by the suspension control current. In addition, the maximum suspension force of the HMB in this study is the theoretical value.

4.2. Selection of the Magnetic Pole Areas

The maximum flux is needed in the air gap when the maximum suspension forces are present in the radial and axial directions.

According to (25),

$$\Phi_{r\max} = \Phi_{a\max} = \Phi_1 = \beta\Phi_r = \beta B_r S_m = \beta\alpha B_r S_{pm} \tag{28}$$

because of the following relationship,

$$\Phi_{r\max} = B_{r\max} \cdot S_{ra},\ \Phi_{a\max} = B_{a\max} \cdot S_{ax} \tag{29}$$

Substituting (29) into (28), after some manipulation, yields:

$$\frac{S_{pm}}{S_{ra}} = \frac{B_{r\max}}{\beta \cdot \alpha \cdot B_r},\ \frac{S_{pm}}{S_{ax}} = \frac{B_{a\max}}{\beta \cdot \alpha \cdot B_r} \tag{30}$$

As the magnitudes of $B_{a\max}$, $B_{r\max}$, α, β and B_r are constant values for a given permanent magnet, we can then select the magnetic pole areas according to (30).

4.3. Electric Loading and Air Gap Length

After some manipulation, substituting (6) into (17) and (18) yields:

$$N_r i_{rs} = \Phi_{cr} \frac{g_1}{\mu_0 S_{ra}},\ N_a i_{ax} = \Phi_{ca} \frac{g_0}{\mu_0 S_{ax}} \tag{31}$$

According to (23) and (24), we can obtain the following equation when the maximum suspension forces are acting on the rotor:

$$N_r i_{rsm} = B_{ra2}\frac{g_1}{\mu_0},\ N_a i_{axm} = B_{ax2}\frac{g_0}{\mu_0} \tag{32}$$

The required ampere-turns $N_r i_{rs}$ and $N_a i_{ax}$ are proportional to g_1 and g_0, respectively. B_{ra2} and B_{ax2} are the magnetic flux densities in the radial and axial directions, respectively, corresponding to Φ_{a2}. i_{rsm} and i_{axm} are the maximum currents in the radial and axial suspension windings, respectively. g_1 and g_0 are set to 1.0 mm in the magnetic bearings.

5. Losses in HBM

The losses in HMB include rotor losses and stator losses. Rotor losses mainly include the air-friction loss and iron loss in the rotor; the stator losses mainly include copper loss caused by the control currents through the windings and iron loss in the stator.

In particular, the air-friction loss on the rotor can be estimated by the equation derived for rotating cylinders, which can be written as:

$$p_{air} = kC_f \pi \rho \omega^3 r l \tag{33}$$

where k is the roughness coefficient, the value is 1.0 for a smooth surface and 2.5 for an axially-slotted surface, ρ is the density of fluid, C_f depends on the radius of rotor, radial air gap length and the Reynolds number, ω is the angular velocity of rotor, l is the length of the rotor and r is the radius of the rotor [27].

The iron losses on the rotor can be divided into the magnetic hysteresis loss and the eddy-current loss. The magnetic hysteresis loss was caused by the difference of the flux density. Meanwhile, the eddy-current loss was caused by the circulation of swirling flow because of the external time-varying magnetic field. The iron losses on the rotor can be written as follows:

$$p_{Fe} = (k_h f_r B_m^{1.6} + \frac{1}{6R}\pi^2 e^2 f_r^2 B_m^2) V_{fe} \tag{34}$$

where k_h is the hysteresis loss coefficient, B_m is the peak flux density, f_r is the operating frequency, R is the unit resistance of the iron core, e is the lamination thickness of the iron core and V_{fe} is the iron core volume, respectively. It can be seen that the rotor core loss mainly depends on the loss factor of core material, the operating frequency and the amplitude of the flux density.

The iron loss in the stator caused by the difference of the flux density and the power amplifiers can be negligible relative to the copper loss in the stator. There are four sets of windings with the maximum number of ampere turns $NI_{r\max}$ in the x and y axis respectively, two sets of windings with the maximum number of ampere turns $NI_{a\max}$ in the z axis. The maximum allowable copper loss in the stator at the full load operation can be written as follows:

$$p_{Cu} = \frac{8\rho_1 l_{mr} {n_r}^2}{A_n K_{st}} i_{r\max}^2 + \frac{2\rho_2 l_{ma} {n_a}^2}{A_n K_{st}} i_{a\max}^2 \tag{35}$$

where ρ_1 is the resistivity of the winding in the x and y axis and ρ_2 is the resistivity of the winding in the z axis. l_{mr}, l_{ma} are the average length of the windings in radial and axial direction, respectively. A_n is the cross-sectional area of the windings, k_{st} is the lamination factor of the stator, $i_{r\max}$, $i_{a\max}$ are the maximum current of the radial and axial direction, respectively. When the HMB operates at rated speed and full load, the FEA-predicted variations of total copper losses and iron losses in this HMB are shown in Figure 7. Additionally, the copper losses in Figure 7 are extreme values because the radial and axial control currents are connected to the windings at the same time. It can be seen that the iron losses are much smaller compared with the copper losses in this HMB.

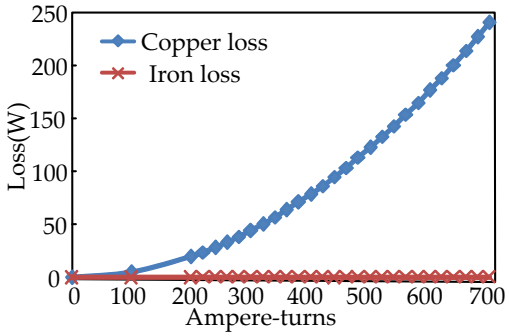

Figure 7. Variation of losses with ampere-turns.

6. FEA, Unbalanced Force versus Displacement and Comparison

6.1. FEA

The key parameters of the proposed HMB used in 5-kW direct-drive wind turbines can be designed based on the structure parameter as shown in Table 1.

Table 1. Key parameters of the proposed HMB.

Parameters	Value
Axial air gap length, g_1, mm	1
Radial air gap length, g_0, mm	1
Height of PM, h_m, mm	10
Maximum number of ampere turns, $N_r i_{rs}$, $N_a i_{ax}$	700
Axial length of outer stator, mm	240
Outer diameter of outer stator, mm	342
Axial length of rotor, mm	120
Outer diameter of rotor, mm	100
Axial length of PM ring, mm	120
Height of the inner stator tooth, mm	70
Width of the inner stator tooth, mm	30
Yokes of inner and outer stator, mm	20
Relative permeability of PM, μ_r	1.1
Remanence for PM, B_r, T	1.25

The finite element analysis (FEA) method, which is based on Maxwell differential equation and adopted the form of discrete, is widely used in various engineering electromagnetic fields. The FEA model of the proposed HMB can be set up based on the parameters given in Table 1. The 3D static magnetic field is used to calculate the magnetic field strength and observe the flux density distribution of the proposed HMB. The transient field is to calculate the force and torque when the rotor is twisted from the equilibrium position. The mesh operations in the proposed HMB are set as follows: the length of the stator and rotor cores are set as 4 mm; the length of the regions of the band and air gap are set as 1.5 mm; the length of control windings is set as 3 mm. The inner stator, outer stator and rotor are made of silicon steel DW360-50; the ring type permanent magnet is NdFeBN42SH. Figure 8 shows the 3D flux density distribution of the PM ring when the rotor is in the center position without eccentricity. Figure 9 presents the flux density distribution of the control windings in the radial and axial directions. Figure 10 shows the flux density distribution when the rotor deviates away from the equilibrium position.

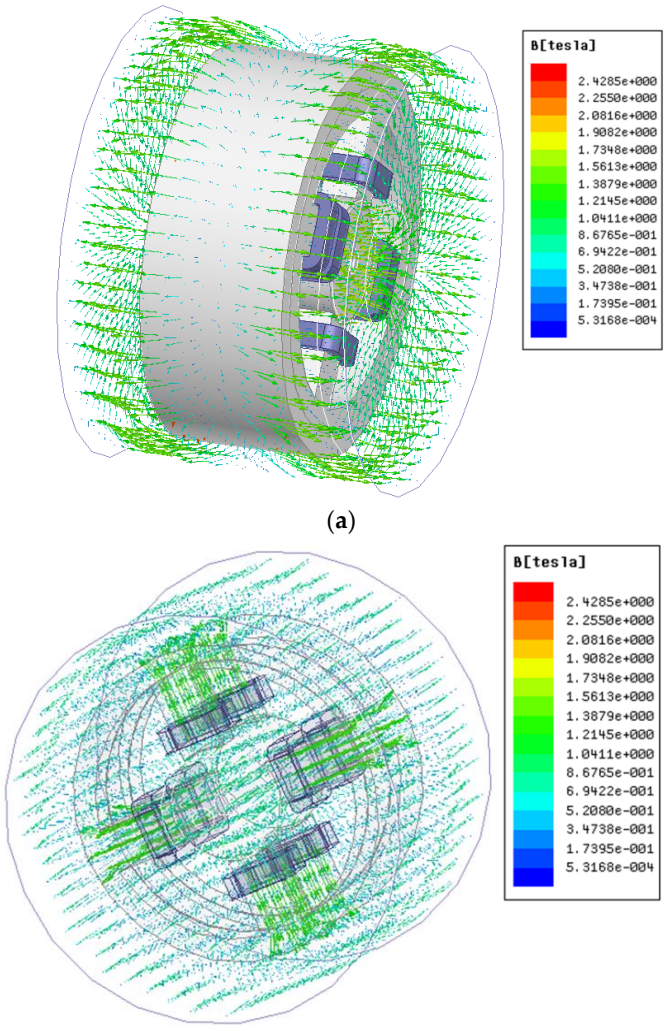

Figure 8. Flux density distribution of the PM ring. (**a**) Flux density distribution of PM ring in the outer stator; (**b**) flux density distribution of PM ring in the inner stator teeth.

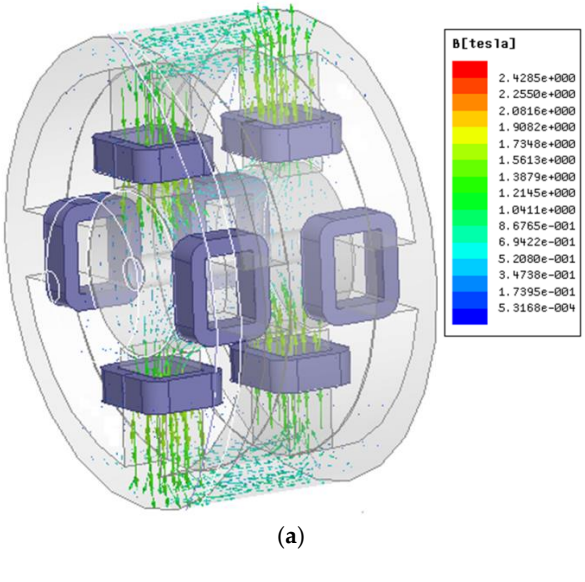

Figure 9. *Cont.*

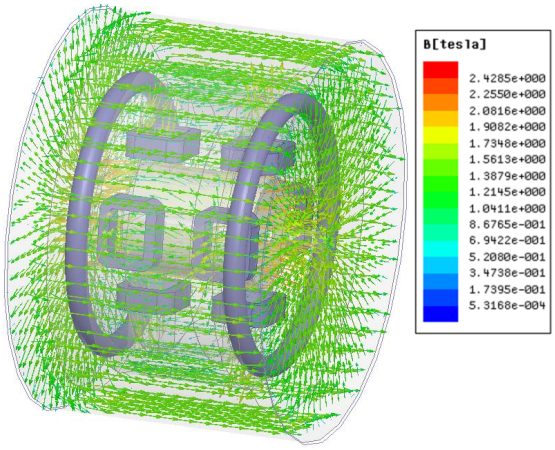

(**b**)

Figure 9. Flux density distribution at rated current. (**a**) Flux density distribution of one set of radial control windings; (**b**) flux density distribution of one set of axial control windings.

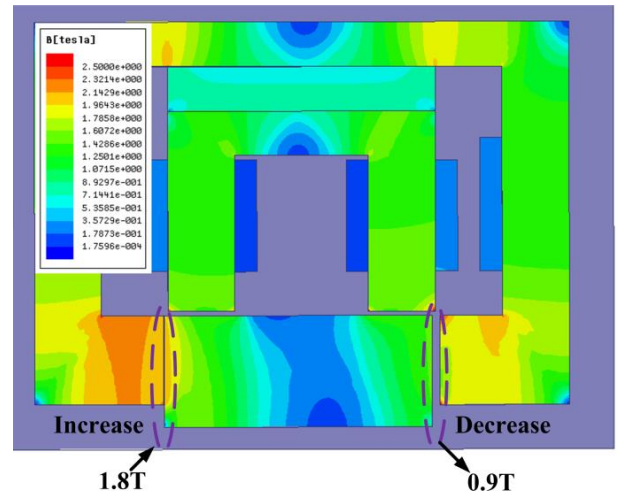

(**a**)

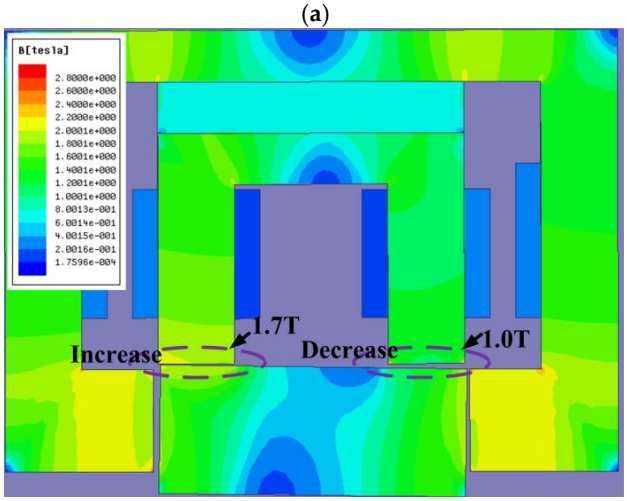

(**b**)

Figure 10. Flux density distribution when the rotor deviates away from the equilibrium position. (**a**) Flux density distribution when the rotor offsets in the axial direction; (**b**) flux density distribution when the rotor twists in the radial direction.

The suspension force in radial and axial direction of the proposed HMB is calculated using the 3D FEA to analyze the validity and accuracy of the accurate equivalent magnetic circuit. As shown in Figure 11, F_{ax} and F_{ra} are the axial and radial suspension forces calculated based on (20) and (21), respectively; F_{n1}, F_{a1} are the radial and axial suspension forces of the HMB proposed in this paper obtained using the FEA; F_{n2}, F_{a2} are the radial and axial suspension forces of the HMB in [23] at the same parameters using FEA. Figure 11 also shows the relation between the axial and radial suspension forces and the ampere-turns when the rotor is at the equilibrium position. The magnitudes of the suspension force are linearly dependent on the ampere-turns. Moreover, the magnitudes of the calculated force based on the magnetic circuit analysis in this study are basically consistent with that of the FEA. The magnitudes of the axial force F_{a2} in [23] are smaller than F_{a1} in this paper, and the magnitudes of F_{n2} are almost the same as F_{n1} in this paper.

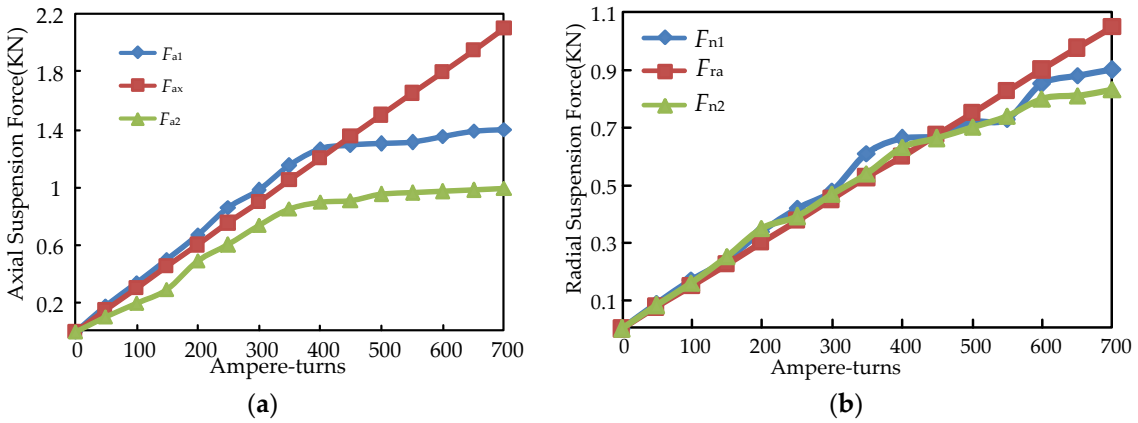

Figure 11. A comparison between the precision equivalent magnetic circuit and two kinds of HMB. (**a**) Axial suspension force versus ampere-turns; (**b**) radial suspension force versus ampere-turns.

6.2. Unbalanced Force versus Displacement in Radial and Axial Directions

The unbalanced force will be occurred as the rotor shifts. The relationship between the offset and the unbalanced force in the axial and radial directions is analyzed in this study. Figure 12 shows the relationship between the axial direction offset z and the axial unbalanced force analyzed with 3D FEA. F_{u1} and F_{u2} are the axial unbalance forces in this paper and in [23], respectively. As shown in Figure 12, the axial unbalanced force F_{u2} in [23] is near the F_{u1} at the smaller offset of the rotor, but F_{u2} is much smaller than F_{u1} at the larger offset of the rotor. Figure 12 further demonstrates that the two unbalanced forces are almost linearly dependent on the axial direction displacement z. The maximum unbalanced force of F_{u1} and F_{u2} in the axial direction are 1150 N and 865 N respectively for the displacement z = 1 mm when the rotor shaft is touched down bearings. Figure 13 illustrates the radial offset angle θ versus the unbalanced force in the radial and axial directions. F_{ru1}, F_{au1} are the radial and axial unbalanced forces of the HMB in this paper, respectively. F_{ru2}, F_{au2} are the radial and axial unbalanced forces in [23]. It also presents that the radial unbalanced forces F_{ru1} and F_{ru2} are almost linearly dependent on the radial offset angle θ. Moreover, the axial unbalanced forces slowly increase according to the radial offset angle θ. The maximum axial unbalanced force F_{au1} is 9.6 N and F_{au2} is 89N when the rotor shaft is deflected at the maximum angle. As shown in Figure 13, the axial unbalance force in [23] is larger than the axial unbalance force in this paper.

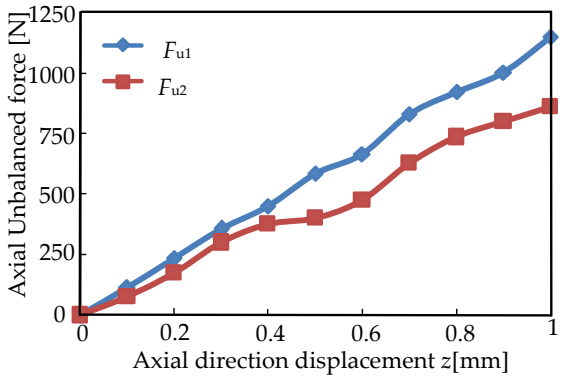

Figure 12. Axial direction displacement versus axial unbalanced force.

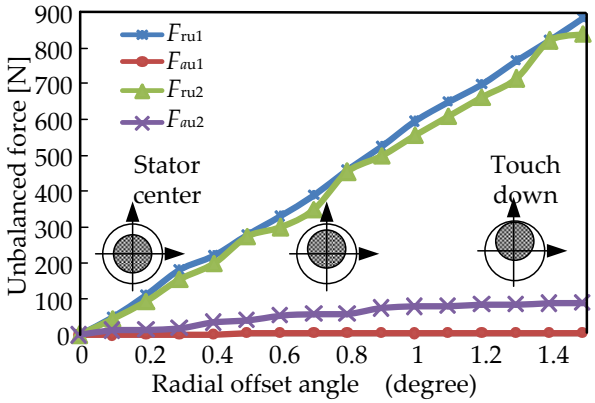

Figure 13. Radial offset angle versus and radial unbalanced force.

7. Conclusions

This study proposes a five-degree-of-freedom hybrid magnetic bearing, which can realize suspension in the four-degree-of-freedom radial and one-degree-of-freedom axial directions. The two-degree-of-freedom suspension in the radial direction can be achieved by only one set of radial control windings. Therefore, only two sets of radial control windings are used in the proposed hybrid magnetic bearing. A cylindrical rotor core without a large thrust disc is used in the novel hybrid magnetic bearing. Accordingly, the system volume, numbers of controller and power amplifier will be reduced in the magnetic levitation system. The precision equivalent magnetic circuit model and the accuracy of the analytical method are validated by the 3D finite element analysis based on the given parameters in Table 1. The prototype of the proposed hybrid magnetic bearing will be presented in the future work based on the model derived in this study.

Acknowledgments: This work was supported by the Priority Academic Program Development of Jiangsu Higher Education Institutions, the Natural Science Foundation of Jiangsu Province (BK20150524) and the Professional Research Foundation for Advanced Talents of Jiangsu University under Project (14JDG131), National Natural Science Foundation of China (51607080).

Author Contributions: Yanjun Yu and Weiyu Zhang are responsible for the theoretical analysis and calculation of the proposed 5-DOF hybrid magnetic bearing. Yanjun Yu and Yuxin Sun are responsible for the finite element analysis of the proposed HMB. Yanjun Yu and Peifeng Xu wrote the paper. All authors read and approved the final manuscript.

Conflicts of Interest: The authors declare no conflict of interest.

References

1. Ouyang, H.; Liu, F.; Zhang, G.M. Vibration suppression for rotor system of magnetic suspended wind turbines using cross-feedback-based sliding mode control. In Proceedings of the IEEE International Symposlum on System Integration, Nagoya, Japan, 11–13 December 2015; pp. 112–115.
2. Muyeen, S.M. *Wind Energy Conversion Systems Technology and Trends*; China Machine Press: Beijing, China, 2013.
3. Zhu, H.; Ding, S.; Jv, J. Modeling for three-pole radial hybrid magnetic bearing considering edge effect. *Energies* **2016**, *9*, 345. [CrossRef]
4. Ding, W.; Liu, L.; Lou, J.Y. Design and control of a high-speed switched reluctance machine with conical magnetic bearings for aircraft application. *IET Electr. Power Appl.* **2012**, *7*, 179–190. [CrossRef]
5. Chow, S.T.; Shyh, L.C. Design and control of a ring-type flywheel battery system with hybrid halbach magnetic bearings. In Proceedings of the IEEE/ASME International Conference on Advanced Intelligent Mechatronics, Besancon, France, 8–11 July 2014; pp. 1558–1562.
6. Ji, L.; Xu, L.X.; Jin, C.W. Research on a low power consumption six-pole heteropolar hybrid magnetic bearing. *IEEE Trans. Magn.* **2013**, *49*, 4918–4926. [CrossRef]
7. Yonmook, P. Design and implementation of an electromagnetic levitation system for active magnetic bearing wheels. *IET Control Theory Appl.* **2014**, *8*, 139–148.
8. Wu, D.; Liu, X.; Zhu, Z.Q.; Pride, A.; Deodhar, R.; Sasaki, T. Switched flux hybrid magnet memory machine. *IET Electr. Power Appl.* **2015**, *9*, 160–170. [CrossRef]
9. Sun, J.; Zhang, Y. A novel integrated structure with a radial displacement sensor and a permanent magnet biased radial magnetic bearing. *Sensors* **2014**, *14*, 1950–1960. [CrossRef] [PubMed]
10. Xu, S.L.; Sun, J.J. Decoupling structure for heteropolar permanent magnet biased radial magnetic bearing with subsidiary air-gap. *IEEE Trans. Magn.* **2014**, *50*, 8300208. [CrossRef]
11. Liu, G.; Mao, K. A novel power failure compensation control method for active magnetic bearings used in high-speed permanent magnet motor. *IEEE Trans. Power.* **2016**, *31*, 4565–4575. [CrossRef]
12. Jiang, K.J.; Zhu, C.S.; Chen, L.L. Unbalance compensation by recursive seeking unbalance mass position in active magnetic bearing-rotor system. *IEEE Trans. Ind. Electron.* **2015**, *62*, 5655–5664.
13. Liu, Ch.; Liu, G. Equivalent damping control of radial twist motion for permanent magnetic bearings based on radial position variation. *IEEE Trans. Ind. Electron.* **2015**, *62*, 6417–6427. [CrossRef]
14. Bachovchin, K.D.; Hoburg, J.F.; Post, R.F. Stable levitation of a passive magnetic bearing. *IEEE Trans. Magn.* **2013**, *49*, 609–617. [CrossRef]
15. Imoberdorf, P.; Nussbaumer, T.; Johann, W. Analysis of a combined radial-axial magnetic bearing for a high-speed system. In Proceedings of the 5th IET International Conference on Power Electronics, Machines and Drives (PEMD), Brighton, UK, 19–21 April 2010.
16. Daoud, M.I.; Abdel-Khalik, A.S.; Massoud, A.; Ahmed, S.; Abbasy, N.H. A design example of an 8-pole radial AMB for flywheel energy storage. In Proceedings of the 2012 20th International Conference on Electrical Machines (ICEM), Marseille, France, 2–5 September 2012; pp. 1153–1159.
17. Zhang, W.Y.; Zhu, H.Q. Precision modeling method specifically for AC magnetic bearings. *IEEE Trans. Magn.* **2013**, *49*, 5543–5553. [CrossRef]
18. Kim, S.H.; Shin, J.W.; Ishiyama, K. Magnetic bearings and synchronous magnetic axial coupling for the enhancement of the driving performance of magnetic wireless pumps. *IEEE Trans. Magn.* **2014**, *50*, 8300208. [CrossRef]
19. Zhang, W.Y.; Zhu, H.Q. Control system design for a five-degree-of-freedom electrospindle supported with AC hybrid magnetic bearings. *IEEE/ASME Trans.* **2015**, *20*, 2525–2537. [CrossRef]
20. Lin, F.J.; Chen, S.Y.; Huang, M.S. Intelligent double integral sliding-mode control for five-degree-of-freedom active magnetic bearing system. *IET Control Theory Appl.* **2011**, *5*, 1287–1303. [CrossRef]
21. Liu, S.; Song, L.; Li, S.; Wang, J.; Lei, X. Decoupling active and passive hybrid axial and radial magnetic bearing. In Proceedings of the 4th International Conference on Control, Automation and Information Sciences (ICCAIS), Changshu, China, 29–31 October 2015; pp. 402–407.
22. Dash, S.K.; Swarup, K.S.; Rajan, K.K. Design optimization of large gap single axis thrust magnetic bearing actuator. *Int. J. Appl. Electromagn. Mech.* **2015**, *47*, 661–675.

23. Wang, G.; Xu, L.X. Structure and magnetic circuit analysis of permanent magnet biased magnetic bearing with five degrees of freedom. *Dev. Innov. Mach. Electr. Prod.* **2003**, *6*, 16–18.
24. Masuzawa, T.; Kojima, J.; Onuma, H. Micro magnetic bearing for an axial flow artificial heart. In Proceedings of the 9th International Symposium on Magnetic Bearings, Lexington, KY, USA, 3–6 August 2004; pp. 89–94.
25. Wang, X.; Fang, J.C.; Fan, Y.H.; Sun, J.J. Axial force tilting permanent-magnet-biased magnetic bearing with five degrees of freedom and magnetic field decoupling design. *Proc. CSEE* **2011**, *31*, 91–98.
26. Schweitzer, G.; Maslen, E.H. *Magnetic Bearings: Theory, Design, and Application to Rotating Machinery*; China Machine Press: Beijing, China, 2012.
27. Nerg, J.; Rilla, M.; Pyrhonen, J. Thermal analysis of radial-flux electrical machines with a high power density. *IEEE Trans. Ind. Electron.* **2008**, *55*, 3543–3554. [CrossRef]